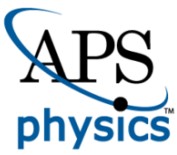

This is the accepted manuscript made available via CHORUS. The article has been published as:

Accessing Phonon Polaritons in Hyperbolic Crystals by Angle-Resolved Photoemission Spectroscopy

Andrea Tomadin, Alessandro Principi, Justin C. W. Song, Leonid S. Levitov, and Marco Polini

Phys. Rev. Lett. **115**, 087401 — Published 21 August 2015

DOI: 10.1103/PhysRevLett.115.087401

Accessing phonon polaritons in hyperbolic crystals by ARPES

Andrea Tomadin,[1] Alessandro Principi,[2] Justin C.W. Song,[3] Leonid S. Levitov,[4,*] and Marco Polini[1,5,†]

[1] *NEST, Istituto Nanoscienze-CNR and Scuola Normale Superiore, I-56126 Pisa, Italy*
[2] *Department of Physics and Astronomy, University of Missouri, Columbia, Missouri 65211, USA*
[3] *Walter Burke Institute for Theoretical Physics and Institute for Quantum Information and Matter, California Institute of Technology, Pasadena, CA 91125, USA*
[4] *Department of Physics, Massachusetts Institute of Technology, Cambridge, Massachusetts 02139, USA*
[5] *Istituto Italiano di Tecnologia, Graphene Labs, Via Morego 30, I-16163 Genova, Italy*

Recently studied hyperbolic materials host unique phonon-polariton (PP) modes. The ultra-short wavelengths of these modes, which can be much smaller than those of conventional exciton-polaritons, are of high interest for extreme sub-diffraction nanophotonics schemes. Polar hyperbolic materials such as hexagonal boron nitride can be used to realize strong long-range coupling between PP modes and extraneous charge degrees of freedom. The latter, in turn, can be used to control and probe PP modes. Of special interest is coupling between PP modes and plasmons in an adjacent graphene sheet, which opens the door to accessing PP modes by angle-resolved photoemission spectroscopy (ARPES). A rich structure in the graphene ARPES spectrum due to PP modes is predicted, providing a new probe of PP modes and their coupling to graphene plasmons.

Introduction.—The intrinsic hyperbolic character [1] of hexagonal boron nitride (hBN) grants a unique platform for realizing deep-subwavelength nanophotonic schemes. Key to these developments are phonon-polariton (PP) modes that exist within *reststrahlen* frequency bands [2, 3], characterized by wavelengths that can be as small as 1-100 nm. Highly directional, these modes exhibit deep sub-diffraction confinement of light with wavelengths far shorter than those of exciton-polaritons in semiconductor microcavities [4]. PPs have been shown to propagate with low losses [2, 3] besting artificial metallic-resonator metamaterial schemes, and opening the door to hyperlensing [5, 6].

Key to harnessing PP modes is gaining access to their response over a wide wavenumber and energy bandwidths. However, to date PPs have only been studied within a small frequency range limited by laser choice (e.g. $167\ \text{meV} \lesssim \hbar\omega \lesssim 198\ \text{meV}$ via scattering-type near-field optical spectroscopy technique [2]), or at specific wavelengths fixed by the sample geometry via Fourier transform infrared spectroscopy of nanofabricated nanopillars [3]. New approaches allowing to resolve the PP modes at shorter wavelengths and over a broad range of energies are therefore highly desirable.

Here we describe an angle-resolved photoemission spectroscopy (ARPES) [9] scheme to achieve broadband energy-resolved access to ultra-short wavelength PPs in hBN. At first glance, ARPES access to PPs in a wide-bandgap insulator (hBN) where no free carriers are available may seem counterintuitive. However, the key to our protocol lies in coupling PPs to charge degrees of freedom in a conductor (e.g. graphene) placed nearby the hyperbolic crystal of interest (hBN), prepared in a slab geometry. Strong coupling [10–15] between hBN Fabry-Pérot PP modes and the collective charge oscillations (i.e. Dirac plasmons [16]) in a doped graphene sheet placed over a hBN slab gives rise to new channels for

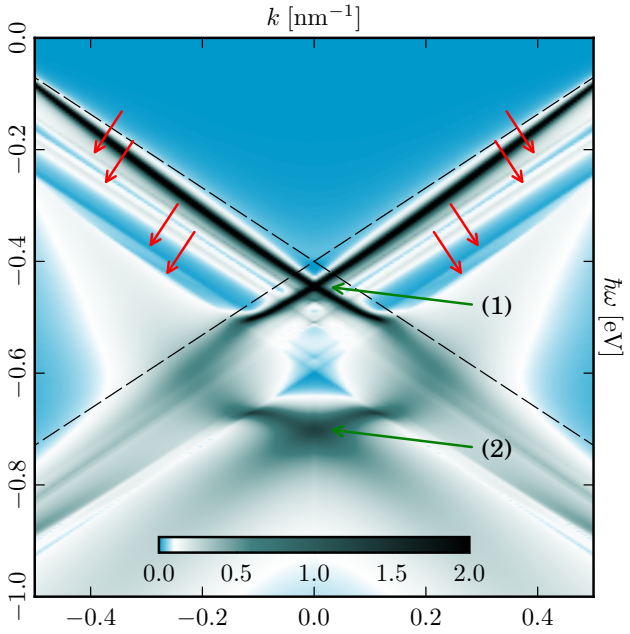

FIG. 1. (Color online) Signatures of PP modes in the quasiparticle spectral function $\mathcal{A}(\boldsymbol{k},\omega)$ of a doped graphene sheet placed over a hBN slab, obtained from Eqs. (3) and (4). Note the black linearly-dispersing quasiparticle bands, which display a clear Dirac crossing labeled by (1), and the broad spectral feature labeled by (2) due to the emission of the plasmon-phonon polariton mode with highest energy in Fig. 2(a). The Fermi energy is positioned at $\omega = 0$. Emission of polariton modes [see Fig. 2(a)] by the holes created by photo-excited electrons gives rise to four dispersive satellite bands running parallel to the main quasiparticle bands (marked by red arrows). The feature (2) is mainly plasmonic,whereas the satellite bands, crossing at $k = 0$ between features (1) and (2), are entirely due to Fabry-Pérot hBN phonon-polariton modes. Parameters used: Fermi energy $\varepsilon_{\rm F} = 400$ meV, hBN slab thickness $d = 60$ nm, $\epsilon_{\rm a} = 1$ (vacuum), $\epsilon_{\rm b} = 3.9$ (SiO_2). The colorbar refers to the values of $\hbar\mathcal{A}(\boldsymbol{k},\omega)$ in eV.

quasiparticle decay yielding a rich structure of dispersive satellite features—marked by red arrows in Fig. 1—in the graphene ARPES spectrum $\mathcal{A}(\boldsymbol{k},\omega)$. Since hBN Fabry-Pérot PPs are controlled by slab thickness, the composite G/hBN structure features a novel ARPES spectrum with features that are highly tunable by thickness.

The greatest practical advantage of this approach is that ARPES achieves extreme resolution over a wide range of wave vectors $\boldsymbol{k}$ (from the corners K, K' of the graphene Brillouin zone to the Fermi wave number $k_{\rm F}$ in graphene) and energies $\hbar\omega$, with all energies below the Fermi energy being probed simultaneously. This gives an additonal benefit, besides tunability, in that the entire range of frequencies and wavenumbers can be covered within a single experiment. It is remarkable that a one-atom-thick conducting material like graphene, once placed over an insulating hyperbolic crystal, enables ARPES studies of PP modes over the full range of wave vectors and energies of interest.

From a more fundamental perspective, ARPES will also be an ideal tool to investigate whether effective electron-electron (e-e) interactions mediated by the exchange of PPs are capable of driving electronic systems towards correlated states. Finally, looking at our results from the point of view of graphene optoelectronics, one can envision situations in which the tunable coupling between graphene quasiparticles and the complex excitations of its supporting substrate can be used to achieve control over the *spectral* properties of graphene carriers, including their decay rates, renormalized velocities, etc. This degree of tunability may have important implications on the performance of graphene-based photodetectors [17].

Phonon and plasmon-phonon polaritons.—We consider a vertical heterostructure—see inset in Fig. 2(b)—composed of a graphene sheet located at $z=0$ and placed over a homogeneous anisotropic insulator of thickness d with dielectric tensor $\hat{\boldsymbol{\epsilon}} = \mathrm{diag}(\epsilon_x, \epsilon_y, \epsilon_z)$. Homogeneous and isotropic insulators with dielectric constants $\epsilon_{\rm a}$ and $\epsilon_{\rm b}$ fill the two half-spaces $z>0$ and $z<-d$, respectively. The Fourier transform $V_{\boldsymbol{q},\omega}$ of the Coulomb interaction potential, as dressed by the presence of a *uniaxial* ($\epsilon_y=\epsilon_x$) dielectric, is given by

$$V_{\boldsymbol{q},\omega} = v_{\boldsymbol{q}} \frac{\sqrt{\epsilon_x\epsilon_z} + \epsilon_{\rm b}\tanh(qd\sqrt{\epsilon_x/\epsilon_z})}{\sqrt{\epsilon_x\epsilon_z} + (\epsilon_x\epsilon_z+\epsilon_{\rm b}\epsilon_{\rm a})\tanh(qd\sqrt{\epsilon_x/\epsilon_z})/(2\bar{\epsilon})}, \tag{1}$$

where $v_{\boldsymbol{q}} = 2\pi e^2/(q\bar{\epsilon})$ with $\bar{\epsilon} = (\epsilon_{\rm a}+\epsilon_{\rm b})/2$ is the ordinary 2D Coulomb interaction potential. A more general equation, which is also valid in the case $\epsilon_y \neq \epsilon_x$, can be found in Sect. I of Ref. 18.

In the case of hBN, the components ϵ_x and ϵ_z of the dielectric tensor have an important dependence on frequency ω in the mid infrared [21]. The simplest parametrization formulas for $\epsilon_{x,z}=\epsilon_{x,z}(\omega)$ are reported in Sect. I of Ref. 18 and have been used for the numerical calculations. More realistic parametrizations can be found in the Supplementary Information of Ref. 13.

Standing PP modes [2] correspond to poles of the dressed interaction $V_{\boldsymbol{q},\omega}$ *inside* the reststrahlen bands. These can be found by looking at the zeroes of the denominator in Eq. (1), $\sqrt{|\epsilon_x(\omega)\epsilon_z(\omega)|} + (2\bar{\epsilon})^{-1}[\epsilon_x(\omega)\epsilon_z(\omega) + \epsilon_{\rm b}\epsilon_{\rm a}]\tan[qd\sqrt{|\epsilon_x(\omega)/\epsilon_z(\omega)|}] = 0$. Illustrative numerical results for $d=10$ nm and $d=60$ nm are reported in Fig. 1 of Ref. 18. Analytical expressions, which are valid for $qd \ll 1$ and $qd \gg 1$, are available [18] in the case in which phonon losses in hBN are neglected. For sufficiently thick hBN slabs, there can be modes with group velocity equal to the graphene Fermi velocity $v_{\rm F}$.

Standing PP modes in a hBN slab couple to Dirac plasmons in a nearby graphene sheet. Such coupling is captured by the random phase approximation (RPA) [22]. In the RPA the interacting electron system is taken to respond as an ideal Fermi gas to the Hartree potential determined by the external charges and by the polarization charges, while local field effects due to exchange and correlations are neglected [22]. We introduce the dynamically screened RPA interaction

$$W_{\boldsymbol{q},\omega} = \frac{V_{\boldsymbol{q},\omega}}{\varepsilon(\boldsymbol{q},\omega)} \equiv \frac{V_{\boldsymbol{q},\omega}}{1 - V_{\boldsymbol{q},\omega}\chi_0(q,\omega)}. \tag{2}$$

Here $\varepsilon(\boldsymbol{q},\omega)$ is the RPA dielectric function and $\chi_0(q,\omega)$ is the density-density response function of a 2D massless Dirac fermion fluid [23]. While the poles of $V_{\boldsymbol{q},\omega}$ physically yield slab PP modes, new poles of $W_{\boldsymbol{q},\omega}$ emerge from electron-phonon interactions. These are weakly-damped solutions $\omega = \Omega_{\boldsymbol{q}} - i0^+$ of the equation $\varepsilon(\boldsymbol{q},\omega)=0$. Illustrative numerical results for $\varepsilon_{\rm F}=400$ meV and $d=60$ nm are shown in Fig. 2(a). (Results for different values of $\varepsilon_{\rm F}$ and d can be found in Sect. III of Ref. 18.) Solid lines represent plasmon-phonon polaritons that emerge from the hybridization between the Dirac plasmon [16] in graphene (dashed line) and standing PP waves in the hBN slab. The solid red lines denote three polariton branches with a strong degree of plasmon-phonon hybridization. On the contrary, black solid lines denote practically unhybridized slab PP modes. We clearly see that there are several plasmon-phonon polariton modes (green circles) with group velocity equal to $v_{\rm F}$. These modes couple strongly to quasiparticles in graphene, as we now proceed to demonstrate.

Quasiparticle decay rates.—An excited quasiparticle with momentum $\boldsymbol{k}$ and energy $\hbar\omega$, created in graphene in an ARPES experiment [24–28], can decay by scattering against electron-hole pairs and collective modes. The decay rate $\hbar/\tau_\lambda(\boldsymbol{k},\omega)$ for these processes can be calculated [22] from the imaginary part of the retarded quasiparticle self-energy $\Sigma_\lambda(\boldsymbol{k},\omega)$, i.e. $\hbar/\tau_\lambda(\boldsymbol{k},\omega) = -2\mathrm{Im}\,[\Sigma_\lambda(\boldsymbol{k},\omega)]$. In the RPA and at zero temperature

we have [29, 30]

$$\mathrm{Im}\left[\Sigma_\lambda(\boldsymbol{k},\omega)\right] = \sum_{\lambda'}\int \frac{d^2\boldsymbol{q}}{(2\pi)^2}\mathrm{Im}\left[W_{\boldsymbol{q},\omega-\xi_{\lambda',\boldsymbol{k}+\boldsymbol{q}}}\right]\mathcal{F}_{\lambda\lambda'} \times\left[\Theta(\hbar\omega-\xi_{\lambda',\boldsymbol{k}+\boldsymbol{q}})-\Theta(-\xi_{\lambda',\boldsymbol{k}+\boldsymbol{q}})\right]. \quad (3)$$

Here $\mathcal{F}_{\lambda\lambda'}\equiv[1+\lambda\lambda'\cos(\theta_{\boldsymbol{k},\boldsymbol{k}+\boldsymbol{q}})]/2$ is the chirality factor [29, 30], $\xi_{\lambda,\boldsymbol{k}}=\lambda\hbar v_{\mathrm{F}}k-\varepsilon_{\mathrm{F}}$ is the Dirac band energy measured from the Fermi energy ε_{F} ($\lambda,\lambda'=\pm1$), and $\Theta(x)$ is the usual Heaviside step function. The quantity $\hbar\omega$ is also measured from the Fermi energy and, finally, $\theta_{\boldsymbol{k},\boldsymbol{k}+\boldsymbol{q}}$ is the angle between $\boldsymbol{k}$ and $\boldsymbol{k}+\boldsymbol{q}$. Eq. (3) reduces to the standard Fermi golden rule when only terms of $\mathcal{O}(V^2_{\boldsymbol{q},\omega})$ are retained. Physically, it describes the decay rate of a process in which an initial state with momentum $\boldsymbol{k}$ and energy $\hbar\omega$ (measured from ε_{F}) decays into a final state with momentum $\boldsymbol{k}+\boldsymbol{q}$ and energy $\xi_{\lambda',\boldsymbol{k}+\boldsymbol{q}}$ (measured from ε_{F}). For $\omega<0$, the self-energy expresses the decay of *holes* created inside the Fermi sea. Fermi statistics requires the final state to be *occupied* so both band indices $\lambda'=\pm1$ are allowed in the case $\varepsilon_{\mathrm{F}}>0$ that we consider here. Since ARPES measures the properties of holes produced in the Fermi sea by photo-ejection, only $\omega<0$ is relevant for this experimental probe in an n-doped graphene sheet.

It is convenient to discuss the main physical features of $\mathrm{Im}\left[\Sigma_\lambda(\boldsymbol{k},\omega)\right]$ for an initial hole state with momentum $\boldsymbol{k}=\boldsymbol{0}$. In this case, the 2D integral in Eq. (3) reduces to a simple 1D quadrature. The initial hole energy is $E_{\mathrm{i}}=\hbar\omega+\varepsilon_{\mathrm{F}}$. The final hole energy is $E_{\mathrm{f}}=\xi_{\lambda',\boldsymbol{q}}+\varepsilon_{\mathrm{F}}=\lambda'\hbar v_{\mathrm{F}}q$. When the difference $\Delta_{\lambda',q}\equiv E_{\mathrm{f}}-E_{\mathrm{i}}$ is equal to the real part of the mode energy $\hbar\Omega_{\boldsymbol{q}}$, the initial hole, which has been left behind after the photo-ejection of an electron, can decay by emitting a plasmon-phonon polariton. Since $\hbar\Omega_{\boldsymbol{q}}>\hbar v_{\mathrm{F}}q$, but $\Delta_{\lambda',q}\leq\hbar v_{\mathrm{F}}q$ for intraband transitions, an initial hole state with $E_{\mathrm{i}}<0$ can decay only into a final hole state with $E_{\mathrm{f}}>0$. In particular, when $d\Omega_{\boldsymbol{q}}/dq=\hbar^{-1}d\Delta_{\lambda',q}/dq=\lambda' v_{\mathrm{F}}$, such decay process is *resonant*. When these conditions are met, the inter-band contribution to $\mathrm{Im}\left[\Sigma_\lambda(\boldsymbol{0},\omega)\right]$ peaks at a characteristic value of ω and $\mathrm{Re}[\Sigma_\lambda(\boldsymbol{0},\omega)]$ changes sign rapidly around that frequency. Within RPA, a satellite quasiparticle emerges [31], which is composed by a hole moving with the same speed of a plasmon-phonon polariton. This is a solution of the Dyson equation, distinct from the ordinary quasiparticle solution that becomes the Landau pole of the one-body Green's function as $k\to k_{\mathrm{F}}$ and $\omega\to0$.

The quantity $\mathrm{Im}\left[\Sigma_\lambda(\boldsymbol{0},\omega)\right]$ is plotted as a function of ω in Fig. 2(b), for $\varepsilon_{\mathrm{F}}=400$ meV and $d=60$ nm. (The dependence of the decay rate on ε_{F} and d is discussed in Sect. III of Ref. 18.) We clearly see several peaks in $\mathrm{Im}\left[\Sigma_\lambda(\boldsymbol{0},\omega)\right]$ for $\hbar\omega<-\varepsilon_{\mathrm{F}}$ ($E_{\mathrm{i}}<0$), which occur at values of $\hbar\omega$ that are in a one-to-one correspondence with the "resonant" plasmon-phonon polaritons, i.e. polaritons with group velocity equal to v_{F}, shown in Fig. 2(a).

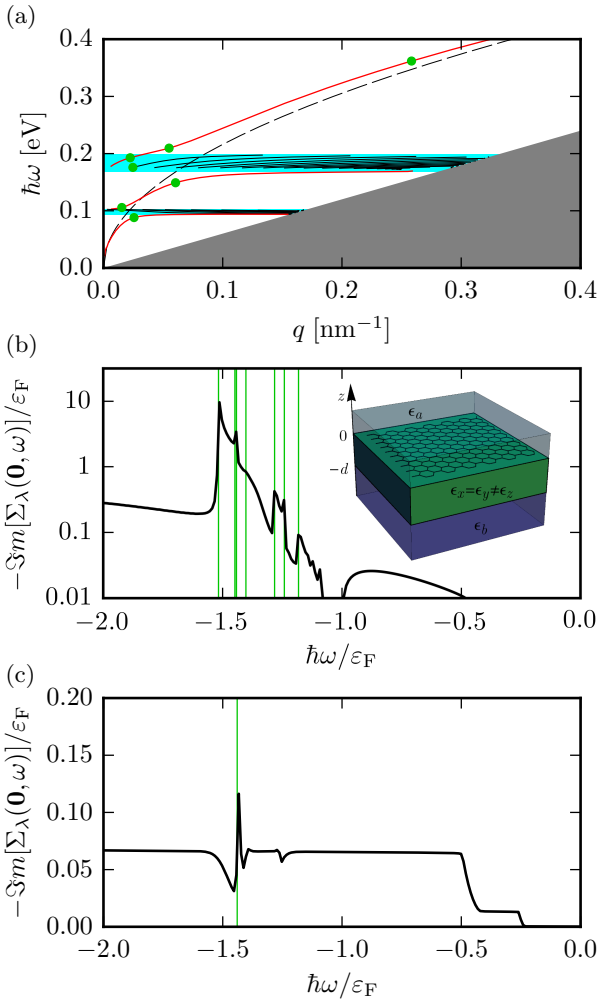

FIG. 2. (Color online) Panel (a) Dispersion relation $\Omega_{\boldsymbol{q}}$ of hybrid plasmon-phonon polaritons (solid lines) with parameters as in Fig. 1. The dashed line represents a Dirac plasmon [16] in graphene, without hBN phonons. Horizontal cyan areas denote the hBN reststrahlen bands. The grey-shaded area represents the intra-band particle-hole continuum in graphene. Green filled circles represent the points where the plasmon-phonon polariton group velocity equals v_{F}. Panel (b) The quantity $-\mathrm{Im}[\Sigma_\lambda(\boldsymbol{k},\omega)]$ (in units of ε_{F} and evaluated at $\boldsymbol{k}=\boldsymbol{0}$) is shown as a function of the rescaled frequency $\hbar\omega/\varepsilon_{\mathrm{F}}$. Green vertical lines denote the values of $\hbar\omega/\varepsilon_{\mathrm{F}}$ at which a plasmon-phonon polariton peak is expected. The inset shows the vertical heterostructure analyzed in this work. Panel (c) Same as in panel (b) but in the absence of e-e dynamical screening; obtained by replacing $W_{\boldsymbol{q},\omega}\to V_{\boldsymbol{q},\omega}$ in Eq. (3). A polaron peak is clearly visible.

Indeed, as stated above, peaks in $\mathrm{Im}\left[\Sigma_\lambda(\boldsymbol{0},\omega)\right]$ are expected at values of $\hbar\omega$—marked by green vertical lines in Fig. 2(b)—given by $\hbar\omega=\hbar v_{\mathrm{F}}q^\star-\varepsilon_{\mathrm{F}}-\hbar\Omega_{\boldsymbol{q}^\star}$, where $q^\star$ is the wave number at which the resonance condition $d\Omega_{\boldsymbol{q}}/dq=v_{\mathrm{F}}$ is satisfied. For example, the resonant mode at highest energy in Fig. 2(a), which occurs at $q^\star\approx0.26$ nm^{-1} and energy $\hbar\Omega_{\boldsymbol{q}^\star}\approx0.36$ eV, yields a peak in $\mathrm{Im}\left[\Sigma_\lambda(\boldsymbol{0},\omega)\right]$ at $\hbar\omega/\varepsilon_{\mathrm{F}}\approx-1.5$, see Fig. 2(b).

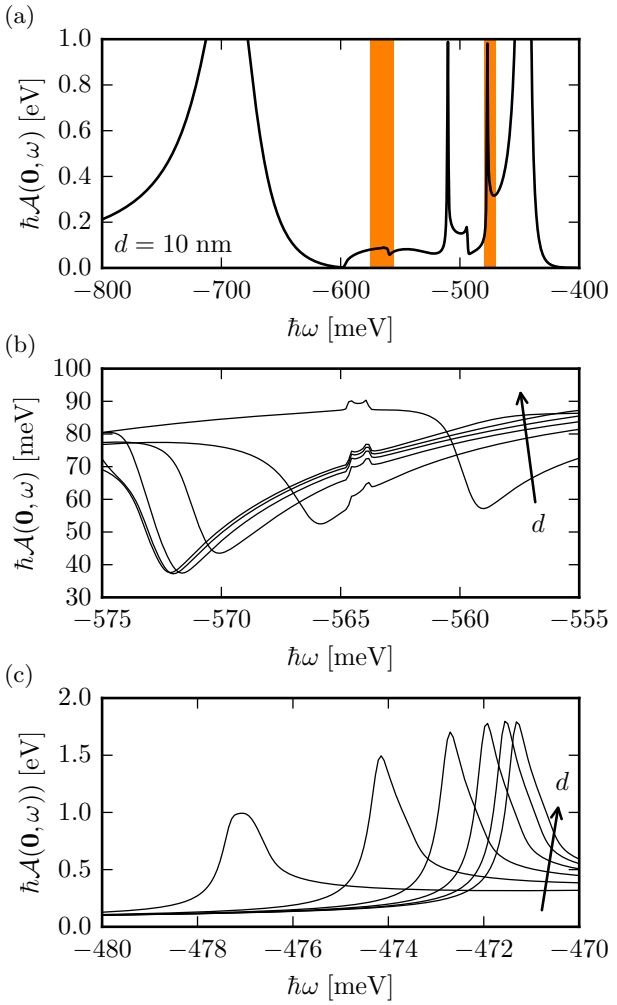

FIG. 3. (Color online) Panel (a) The quasiparticle spectral function $\mathcal{A}(\boldsymbol{k},\omega)$, evaluated at $|\boldsymbol{k}| = 10^{-3}\ k_{\rm F}$, for $d = 10$ nm. The other parameters are as in Fig. 1. Panels (b) and (c) Dependence on the hBN slab thickness d of the spectral function features highlighted by vertical orange-shaded regions in panel (a). Different curves correspond to values of d on a uniform mesh from $d = 10$ nm to $d = 60$ nm.

Comparing Fig. 2(b) with Fig. 2(c), we clearly see the role of dynamical screening due to e-e interactions in graphene. For $\varepsilon(\boldsymbol{k},\omega) = 1$, the off-shell decay rate $\mathrm{Im}\,[\Sigma_\lambda(\mathbf{0},\omega)]$ shows only a polaron peak, due to the emission of a Fabry-Perót PP mode with group velocity equal to $v_{\rm F}$, see Fig. 1 in Ref. 18.

At $\boldsymbol{k} \neq \mathbf{0}$, the conduction and valence band $\mathrm{Im}[\Sigma_\lambda(\boldsymbol{k},\omega)]$ plasmon-phonon polariton peaks broaden and separate, because of [29] the dependence on scattering angle of $\xi_{\lambda',\boldsymbol{k}+\boldsymbol{q}}$ and the chirality factor $\mathcal{F}_{\lambda\lambda'}$, which emphasizes $\boldsymbol{k}$ and $\boldsymbol{q}$ in nearly parallel directions for conduction band states and $\boldsymbol{k}$ and $\boldsymbol{q}$ in nearly opposite directions for valence band states. As a result, the conduction band plasmon-phonon polariton peak moves up in energy while the valence band peak moves down.

Quasiparticle spectral function.—An ARPES experiment [9] probes the quasiparticle spectral function $\mathcal{A}(\boldsymbol{k},\omega) = -\pi^{-1}\sum_\lambda \mathrm{Im}[G_\lambda(\boldsymbol{k},\omega)] = \sum_{\lambda=\pm1}\mathcal{A}_\lambda(\boldsymbol{k},\omega)$. Here $G_\lambda(\boldsymbol{k},\omega)$ is the one-body Green's function in the band representation and

$$\mathcal{A}_\lambda = -\frac{1}{\pi}\frac{\mathrm{Im}\Sigma_\lambda}{(\omega - \xi_{\lambda,\boldsymbol{k}}/\hbar - \mathrm{Re}\Sigma_\lambda/\hbar)^2 + (\mathrm{Im}\Sigma_\lambda/\hbar)^2}\ . \quad (4)$$

The real part $\mathrm{Re}[\Sigma_\lambda(\boldsymbol{k},\omega)]$ of the quasiparticle self-energy can be calculated, at least in principle, from the Kramers-Kronig transform of $\mathrm{Im}[\Sigma_\lambda(\boldsymbol{k},\omega)]$. A more convenient way to handle the numerical evaluation of $\mathrm{Re}[\Sigma_\lambda(\boldsymbol{k},\omega)]$ is to employ the Quinn-Ferrell line-residue decomposition [32].

Our main results for the quasiparticle spectral function $\mathcal{A}(\boldsymbol{k},\omega)$ are summarized in Fig. 1 and Fig. 3. We clearly see that the presence of the hBN substrate is responsible for the appearance of a family of sharp dispersive satellite features associated with the presence of PPs and plasmon-phonon polaritons. This is particularly clear in the one-dimensional cut at $\boldsymbol{k} = \mathbf{0}$ of $\mathcal{A}(\boldsymbol{k},\omega)$ displayed in Fig. 3(a) for $d = 10$ nm. All the sharp structures between the ordinary quasiparticle peak slightly below $\hbar\omega = -0.4$ eV and the peak at $\hbar\omega \approx -0.7$ eV, which is mostly plasmonic in nature, are sensitive to the detailed distribution and dispersion of Fabry-Perót PP in the hBN slab, and therefore to the slab thickness d. This is clearly shown in Fig. 3(b) and (c), where we see shifts of these peaks of several meV, when d is changed from $d = 10$ nm to $d = 60$ nm, while keeping $\varepsilon_{\rm F}$ constant.

In summary, we have studied the coupling between standing phonon-polariton modes in a hyperbolic crystal slab and the plasmons of the two-dimensional massless Dirac fermion liquid in a nearby graphene sheet. We have shown that this coupling yields a complex spectrum of (plasmon-phonon) polaritons, see Fig. 2(a). Plasmon-phonon polaritons with group velocity equal to the graphene Fermi velocity couple strongly with graphene quasiparticles, enabling ARPES access to PP modes in hyperbolic crystal slabs, as shown in Figs. 1 and 3. Recent progress [33] in the chemical vapor deposition growth of large-area graphene/hBN stacks on Cu(111) in ultrahigh vacuum and the ARPES characterization of the resulting samples makes us very confident on the observability of our predictions. In passing, we would like to remark that plasmon-related satellite spectral features tend to be quite robust to disorder [30], as experimentally demonstrated in Ref. [26]. Our findings suggest that appropriate coupling of graphene to substrates which allow strong plasmon-phonon hybridization could open the route to the manipulation of carriers' spectral properties, paving the way for novel device functionalities.

Acknowledgements.—We gratefully acknowledge F.H.L. Koppens for useful discussions. This work was supported by the EC under the Graphene Flagship program (contract no. CNECT-ICT-604391) (A.T. and M.P.), MIUR

(A.T. and M.P.) through the programs "FIRB - Futuro in Ricerca 2010" - Project "PLASMOGRAPH" (Grant No. RBFR10M5BT) and "Progetti Premiali 2012" - Project "ABNANOTECH", the U.S. Department of Energy under grant DE-FG02-05ER46203 (A.P.), and a Research Board Grant at the University of Missouri (A.P.). Work at MIT was supported as part of the Center for Excitonics, an Energy Frontier Research Center funded by the U.S. Department of Energy, Office of Science, Basic Energy Sciences under Award No. desc0001088. This work was also supported, in part, by the U.S. Army Research Laboratory and the U.S. Army Research Office through the Institute for Soldier Nanotechnologies, under contract number W911NF-13-D-0001. Free software (www.gnu.org, www.python.org) was used.

* levitov@mit.edu
† marco.polini@icloud.com

[1] A. Poddubny, I. Iorsh, P. Belov, and Y. Kivshar, Nature Photon. **7**, 948 (2013).
[2] S. Dai, Z. Fei, Q. Ma, A.S. Rodin, M. Wagner, A.S. McLeod, M.K. Liu, W. Gannett, W. Regan, K. Watanabe, T. Taniguchi, M. Thiemens, G. Dominguez, A.H. Castro Neto, A. Zettl, F. Keilmann, P. Jarillo-Herrero, M.M. Fogler, and D.N. Basov, Science **343**, 1125 (2014).
[3] J.D. Caldwell, A. Kretinin, Y. Chen, V. Giannini, M.M. Fogler, Y. Francescato, C.T. Ellis, J.G. Tischler, C.R. Woods, A.J. Giles, M. Hong, K. Watanabe, T. Taniguchi, S.A. Maier, and K.S. Novoselov, Nature Commun. **5**, 5221 (2014).
[4] T. Byrnes, N.Y. Kim, and Y. Yamamoto, Nature Phys. **10**, 803 (2014).
[5] P. Li, M. Lewin, A.V. Kretinin, J.D. Caldwell, K.S. Novoselov, T. Taniguchi, K. Watanabe, F. Gaussmann, and T. Taubner, arXiv:1502.04093.
[6] S. Dai, Q. Ma, T. Andersen, A.S. McLeod, Z. Fei, M. K. Liu, M. Wagner, K. Watanabe, T. Taniguchi, M. Thiemens, F. Keilmann, P. Jarillo-Herrero, M.M. Fogler, and D.N. Basov, arXiv:1502.04094.
[7] F. Keilmann and R. Hillenbrand, Phil. Trans. R. Soc. Lond. A **362**, 787 (2004).
[8] N. Ocelic, A. Huber and R. Hillenbrand, Appl. Phys. Lett. **89**, 101124 (2006).
[9] A. Damascelli, Z. Hussain, and Z.-X. Shen, Rev. Mod. Phys. **75**, 473 (2003).
[10] B. Amorim, J. Schiefele, F. Sols, and F. Guinea, Phys. Rev. B **86**, 125448 (2012).
[11] V.W. Brar, M.S. Jang, M. Sherrott, S. Kim, J.J. Lopez, L.B. Kim, M. Choi, and H. Atwater, Nano Lett. **14**, 3876 (2014).
[12] A. Principi, M. Carrega, M.B. Lundeberg, A. Woessner, F.H.L. Koppens, G. Vignale, and M. Polini, Phys. Rev. B **90**, 165408 (2014).
[13] A. Woessner, M.B. Lundeberg, Y. Gao, A. Principi, P. Alonso-González, M. Carrega, K. Watanabe, T. Taniguchi, G. Vignale, M. Polini, J. Hone, R. Hillenbrand, and F.H.L. Koppens, Nature Mater. **14**, 421 (2015).
[14] S. Dai, Q. Ma, S.-E. Zhu, M. K. Liu, T. Andersen, Z. Fei, M. Goldflam, M. Wagner, K. Watanabe, T. Taniguchi, M. Thiemens, F. Keilmann, G.C.A.M. Janssen, P. Jarillo-Herrero, M.M. Fogler, and D.N. Basov, arXiv:1501.06956.
[15] A. Kumar, T. Low, K.H. Fung, P. Avouris, and N.X. Fang, arXiv:1502.04672.
[16] For reviews on graphene plasmons see e.g. A.N. Grigorenko, M. Polini, and K.S. Novoselov, Nature Photon. **6**, 749 (2012); T. Low and P. Avouris, ACS Nano **8**, 1086 (2014).
[17] F.H.L. Koppens, T. Mueller, Ph. Avouris, A.C. Ferrari, M.S. Vitiello, and M. Polini, Nature Nanotech. **9**, 780 (2014).
[18] See Supplemental Material, which includes Refs. 19 and 20, where we present analytical details on the phonon-polariton dispersion and further numerical results on the quasiparticle decay rates and spectral function.
[19] L.D. Landau and E.M. Lifshitz, *Course of Theoretical Physics: Electrodynamics of Continuos Media* (Pergamon, New York, 1984).
[20] L.V. Keldysh, Pis'ma Zh. Eksp. Teor. Fiz. **29**, 716 (1979).
[21] R. Geick, C. H. Perry, and G. Rupprecht, Phys. Rev. **146**, 543 (1966).
[22] G.F. Giuliani and G. Vignale, *Quantum Theory of the Electron Liquid* (Cambridge University Press, Cambridge, 2005).
[23] B. Wunsch, T. Stauber, F. Sols, and F. Guinea, New J. Phys. **8**, 318 (2006); E.H. Hwang and S. Das Sarma, Phys. Rev. B **75**, 205418 (2007); A. Principi, M. Polini, and G. Vignale, Phys. Rev. B **80**, 075418 (2009).
[24] A. Bostwick, T. Ohta, T. Seyller, K. Horn, and E. Rotenberg, Nature Phys. **3**, 36 (2007).
[25] S.Y. Zhou, G.-H. Gweon, A.V. Fedorov, P.N. First, W.A. der Heer, D.-H. Lee, F. Guinea, A.H. Castro Neto, and A. Lanzara, Nature Mater. **6**, 770 (2007).
[26] A. Bostwick, F. Speck, T. Seyller, K. Horn, M. Polini, R. Asgari, A.H. MacDonald, and E. Rotenberg, Science **328**, 999 (2010).
[27] A.L. Walter, A. Bostwick, K.-J. Jeon, F. Speck, M. Ostler, T. Seyller, L. Moreschini, Y.J. Chang, M. Polini, R. Asgari, A.H. MacDonald, K. Horn, and E. Rotenberg, Phys. Rev. B **84**, 085410 (2011).
[28] D.A. Siegel, C.-H. Park, C. Hwang, J. Deslippe, A.V. Fedorov, S.G. Louie, and A. Lanzara, Proc. Natl. Acad. Sci. (USA) **108**, 11365 (2011).
[29] M. Polini, R. Asgari, G. Borghi, Y. Barlas, T. Pereg-Barnea, and A.H. MacDonald, Phys. Rev. B **77**, 081411(R) (2008).
[30] E.H. Hwang and S. Das Sarma, Phys. Rev. B **77**, 081412(R) (2008).
[31] B.I. Lundqvist, Phys. Kondens. Mater. **6**, 193 (1967); Phys. Kondens. Mater. **6**, 206 (1967); Phys. Kondens. Mater. **7**, 117 (1968); L. Hedin, B.I. Lundqvist, and S. Lundqvist, Solid State Commun. **5**, 237 (1967). It has been claimed [J. Lischner, D. Vigil-Fowler, and S.G. Louie, Phys. Rev. Lett. **110**, 146801 (2013)] that these additional solutions of the Dyson equation disappear when one goes beyond RPA. However, it has been shown that the decay rate and the spectral function still display peaks associated with the collective modes of the electron liquid.
[32] J.J. Quinn and R.A. Ferrell, Phys. Rev. **112**, 812 (1958).
[33] S. Roth, F. Matsui, T. Greber, and J. Osterwalder, Nano

Lett. **13**, 2668 (2013).